Available online at www.sciencedirect.com

jmr&t Journal of Materials Research and Technology

https://www.journals.elsevier.com/journal-of-materials-research-and-technology

Original Article

Influence of manganese on deformation behavior of lightweight steel at different strain rate

Zhongping He[a], *Hongyu Yang*[b], *Yanlin He*[b,*], *Weisen Zheng*[b], *Zhongwei Guan*[a,c], *Lin Li*[b]

[a] *School of Mechanical Engineering, Chengdu University, Chengdu, 610106, China*
[b] *School of Materials Science and Engineering, Shanghai University, Shanghai, 200072, China*
[c] *School of Engineering, University of Liverpool, Liverpool, L69 3GQ, UK*

ARTICLE INFO

Article history:
Received 28 November 2019
Accepted 3 August 2020
Available online 27 August 2020

Keywords:
Strain rate
Manganese content
Deformation behavior
Lightweight steel
Retained austenite

ABSTRACT

Tensile deformation behavior of Fe–0.25C–3.5(10)Mn–5Al lightweight steel was studied in a large range of strain rate (0.001–1200 s^{-1}) by using a universal material testing machine, intermediate strain rate tensile testing apparatus and rotation disk bar-bar tensile impact apparatus. Microstructures of the two steels before and after tension were observed by means of Optical Microscope (OM), Scanning Electron Microscope (SEM), X-ray diffraction (XRD) and Transmission Electron Microscope (TEM). The results show that the two lightweight steels have a high strength and plasticity and exhibit excellent combinations of specific strength and ductility at the strain-rate of 0.001 s^{-1} after annealing at 850 °C for 5 min then directly quenching into water. During the tensile deformation process, the austenite in 3.5 Mn steel is transformed to α′-martensite. While in 10 Mn steel, the austenite is transformed to twinning. With an increase in strain rate from 0.001 to 1200 s^{-1}, tensile strength of the two steels increase, whilst the elongation initially decrease, and then increase. At the strain-rate of 450 s^{-1}, the elongation of the two lightweight steels are minimal, and the energy absorption capacity are the lowest. With the deformation progresses, the value of n increases from small to large, the strain hardening effect becomes high. Uniform deformation of 10 Mn lightweight steel was suppressed at high strain-rate. Comparing with 10 Mn lightweight steel, the austenite in 3.5 Mn lightweight steel is obviously unstable and cannot provide progressive phase transition.

1. Introduction

Stringent regulations of automotive industry to reduce weight and improve crashworthiness has led to the development of a new generation of advanced high-strength steel (AHSS). The first idea was to develop steel with aluminium in order to reduce the material's density [1]. However, the addition of Al drastically decreases Young's modulus of the material [2]. Aluminium is an α-phase former, its solubility in γ-phase is low and fully ferritic steels often show low ductility. Moreover, aluminium enhances microstructure ordering, which often leads to embrittlement problems [3]. The idea of Mn addition was presented to decrease the negative influence of aluminium [4]. Lightweight steel with Al content greater than 3% and Mn

* *Corresponding author.*
E-mail: ylhe@t.shu.edu.cn (Y. He).
https://doi.org/10.1016/j.jmrt.2020.08.020

content below 10% shows great potential as a strong candidate for the third generation AHSS because its high strength ductility exceeds that of the first generation AHSS, and the cost may be lower compared to high Mn second generation AHSS [5–9]. The development of lightweight steel relies on a comprehensive understanding of the relationship between alloying elements, thermomechanical processing, microstructure and mechanical properties [10,11].

Previous studies of such steels have focused on the microstructure evolution during critical annealing processes and their effects on tensile properties [12–15]. And most of the studies were concentrated on the mechanical behavior and microstructure change of lightweight steels under static tension loading conditions. However, the automobile steel body parts are manufactured by forming with the deformation rate in the process being between 10^{-1} and $10\,s^{-1}$. The deformation rate of the material during the impact on the vehicle is in the range of 10^2 to $10^3\,s^{-1}$. Therefore, in order to utilize more lightweight steels in automobiles effectively, it is necessary to understand its mechanical behavior and microstructure evolution under high-speed deformation conditions.

As an important alloying element in lightweight steel, manganese plays an important role in expanding the austenite phase area, lowering the martensite transformation temperature, and improving the stability of austenite. At the same time, the Mn content also affects the magnitude of stacking fault energy, which in turn affects the deformation mechanism and work hardening behavior of lightweight steel. But the studies on dynamic deformation of Fe–C–Mn–Al system steels were mainly focused on high Mn TWIP steels [16–19]. Rahman et al. [16] studied the dynamic behavior of Fe–15Mn–2Si–2Al–0.7C TWIP steel, and indicated that the yield stress increased with an increase in strain rate from 0.01 to $950\,s^{-1}$. Park et al. [17] investigated the quasi-static and dynamic deformation mechanism of Fe–15Mn–1.2Al–0.6C TWIP steel, and demonstrated that the TWIP steel showed a higher strength and similar ductility under dynamic loading because of favorable effect of the increased planar slip and twinning on tensile properties. Tang et al. [18] studied microstructure and mechanical properties of Fe–0.07C–23Mn–3.1Si–2.8Al steel in the strain rate range of $10\,s^{-1}$ to $1000\,s^{-1}$, and the strength and elongation were reported to increase with the increase of strain rate. This is mainly due to strain induced intermediate ε-martensite and intersecting deformed twinning generated under dynamic loading. Ha et al. [19] pointed out that under high strain rate deformation, nanostructured austenite is formed in Fe–22Mn–0.4C TWIP steel due to deformation twinning to form nanoscale twin/substrate sheets, and then dynamic recovery which are caused by adiabatic heating. However, up to date there are relatively few studies on the low Mn lightweight steels, especially in high strain-rate conditions. Considering the complexity of the influence of strain-rate and the Mn content on the deformation behavior and mechanical properties of lightweight steels, the deformation mechanisms of lightweight steels during dynamic deformation are not clear. Therefore, it is necessary to study the influence of strain-rate and Mn content on the dynamic behavior of lightweight steels.

In this study, two new type of low Mn lightweight steels have been designed. The addition of Al reduces the density of the steel. The current work is to explore micro-structural evolution, mechanical properties and deformation behavior of Fe–3.5(10)Mn–5Al–0.25C lightweight steel under the loading in a range of strain-rates ($0.001–1200\,s^{-1}$), to understand the effects of strain-rate and Mn content on adiabatic temperature rise, stacking fault energy(SFE), deformation mechanisms, and mechanical properties of the lightweight steel.

2. Experimental procedure

2.1. Experimental material

The chemical compositions of the steel investigated in the present work are listed in Table 1.

A 150 kg ingot was produced in a vacuum induction melting furnace filled with argon, followed by hot rolling to a thickness of 3.5 mm between 900 °C and 1050 °C, subsequently holding at 650 °C for 1 h and cold rolling to 1.2 mm. In order to obtain the optimal mechanical properties, the two lightweight steel sheets were annealed at 850 °C for 5 min, then directly quenched into water. The density of these steel specimens, measured by the Archimedes Drainage Method, showed a reduction of 7.5% (3.5 Mn) and 7.8% (10 Mn) in comparison to the conventional high strength steel ($7.85\,g/cm^3$).

2.2. Tensile test

The quasi-static tensile properties were measured by MTS809 universal material testing machine at the strain-rate of $10^{-3}\,s^{-1}$. The specimens were designed as shown in Fig. 1. The tensile properties at the strain-rate of $5\,s^{-1}$ were studied using an intermediate strain-rate tensile testing apparatus [20]. The schematic diagrams of the apparatus and the tensile specimen were presented in Fig. 2. The tensile testing at the strain-rate range of $450\,s^{-1}$ and $1200\,s^{-1}$ were performed by using a dynamic tensile testing apparatus [21]. Fig. 3 shows the schematic diagrams of the rotation disk bar-bar tensile impact apparatus and the corresponding tensile specimen. Three samples were used as repetitions in each set of experiments.

2.3. Microstructure observation

The specimens were polished and etched in a solution of 4% Nital. The microstructure observation was conducted by using an optical microscope (Nikon MA100) and a scanning electron microscope (Hitachi S-570). X-ray diffraction (D/MAX-2500) operating at 40 kV and 40 mA was also carried out to identify phases, using Cu Kα radiation (scan rate 2°/min, scan step size 0.02°). The volume fraction of austenite (V_γ) was calculated by Eq. (1) according to Dyson [22].

$$V_\gamma = \frac{1.4I_\gamma}{I_\alpha + 1.4I_\gamma} \quad (1)$$

where I_γ is the average intensity of 220_γ and 331_γ diffraction peaks and I_α is the intensity of 211_α diffraction peak. High resolution transmission electron microscope (JEM-2010 F) was operated at an acceleration voltage of 200 kV. TEM samples

Table 1 – Chemical composition (wt.%) and heat treatment process of the steel tested.

Steel	C	Mn	Al	Fe	Heat treatment process
3.5 Mn	0.25	3.5	5	Bal.	850 °C × 5 min + water quenching
10 Mn	0.25	10	5	Bal.	850 °C × 5 min + water quenching

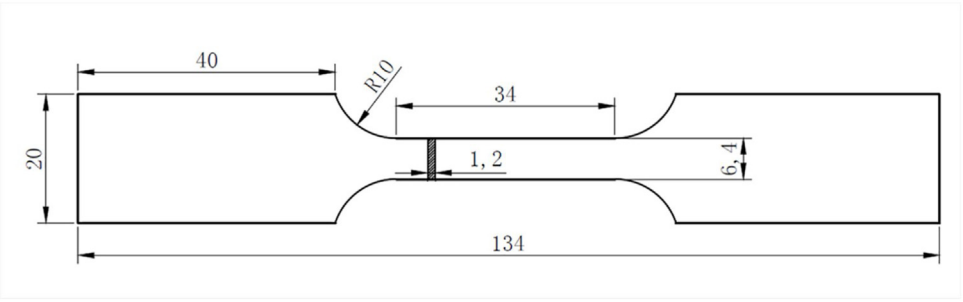

Fig. 1 – Dimensions of the quasi-static tensile specimen with a thickness of 1.2 mm.

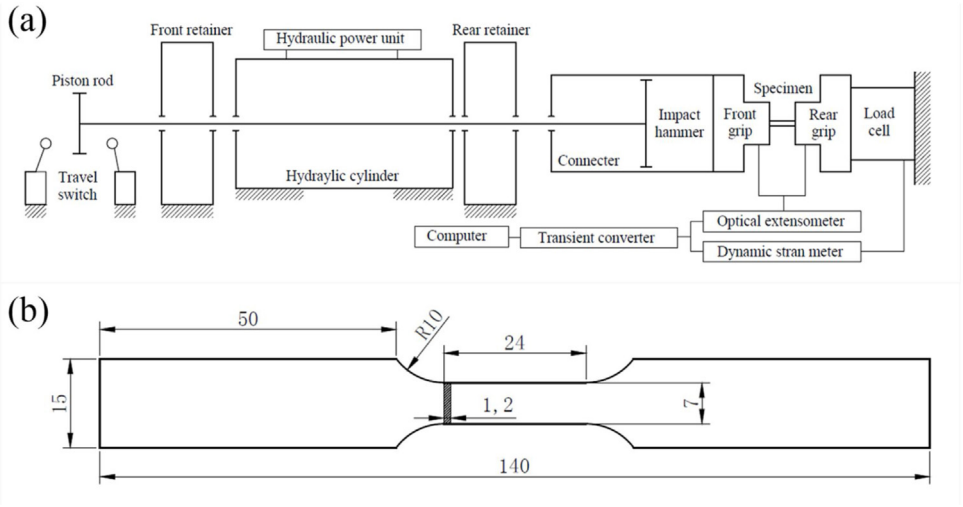

Fig. 2 – Intermediate strain rate material testing: (a) Schematic diagram of apparatus; (b) Dimensions of specimens with a thickness of 1.2 mm.

were cut into 3 mm diameter discs and mechanically polished to 50 μm. Electro polishing was conducted using 5 vol.% perchloric acid in ethanol at −30 °C in a twin jet electro polisher, with the electrical potential being set at 40 V.

3. Results and discussion

3.1. *Microstructure*

Fig. 4(a) and (b) is the optical structure of the steel investigated. The ferrite is white, the austenite is gray or brown. It shows a typical strip-shaped microstructure. In Fig. 4(a), dark gray austenite embedded in white ferrite matrix. In Fig. 4(b), the amount of austenite is more than that of ferrite, and the ferrite embedded in austenite. The microstructure observed by SEM is shown in Fig. 4(c) and (d). In Fig. 4(c), the island-like austenite is observed in ferrite matrix. In Fig. 4(d), most of the austenite is distributed in a band shape, and a small amount of austenite is distributed in the ferrite in an island shape. Combined with quantitative metallography and X-ray diffraction analysis, the microstructure of the 3.5 Mn lightweight steel is composed of 82% of ferrite and 18% of austenite, and the microstructure of the 10 Mn lightweight steel is composed of 45% of ferrite and 55% of austenite. As the manganese content increases, the volume fraction of austenite content increases.

3.2. *Tensile properties of the steel under quasi-static loading conditions*

Fig. 5 presents the room-temperature engineering stress-strain curve of the two lightweight steels at a strain-rate of 0.001 s^{-1}, from which tensile properties are summarized in Table 2. From the figure, it can be seen that the yield strength of 3.5 Mn lightweight steel is 640 MPa, the ultimate tensile strength value is 820 MPa and elongation is 40%. The product of strength and elongation (PSE) of 3.5 Mn steel is 32,800 MPa %. We also can see that the yield strength of 10 Mn lightweight

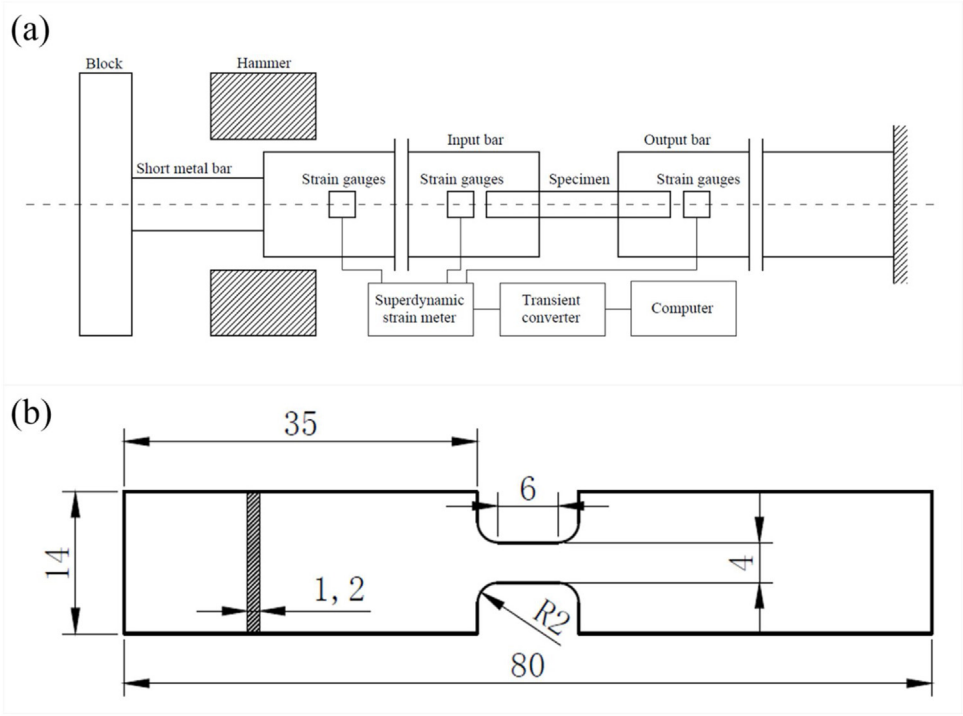

Fig. 3 – Dynamic tensile specimen: (a) Sketch of rotation disk bar–bar tensile impact apparatus; (b) Dimensions of specimens with a thickness of 1.2 mm.

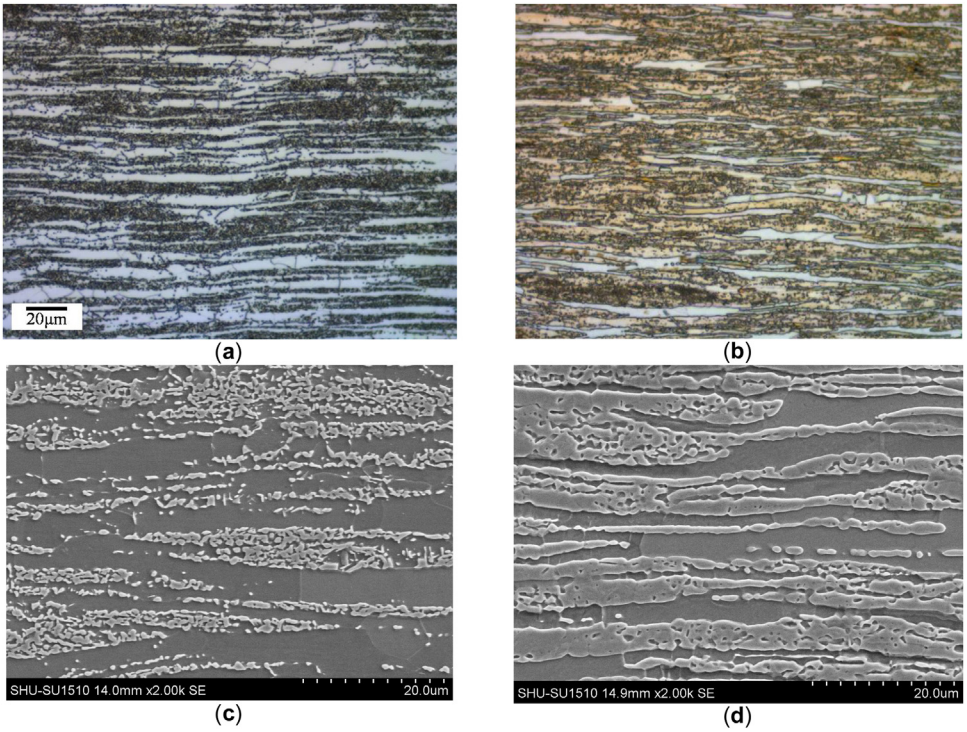

Fig. 4 – Microstructure under: (a) OM micrograph of 3.5 Mn steel; (b) OM micrograph of 10 Mn steel; (c) SEM micrograph of 3.5 Mn steel; (d) SEM micrograph of 10 Mn steel.

steel is 570 MPa, the ultimate tensile strength value is 750 MPa and elongation is 44%. The product of strength and elongation (PSE) of 10 Mn steel is 33,000 MPa %. The two lightweight steels have a high strength and plasticity and exhibits excellent combinations of specific strength and ductility. The increase in manganese content leads to an increase in the volume fraction

Table 2 – Mechanical properties under quasi-static condition of the lightweight steel.

Specimen	Yield strength (MPa)	Ultimate tensile strength (MPa)	Elongation (%)	PSE (MPa %)
3.5 Mn	640	820	40	32,800
10 Mn	570	750	44	33,000

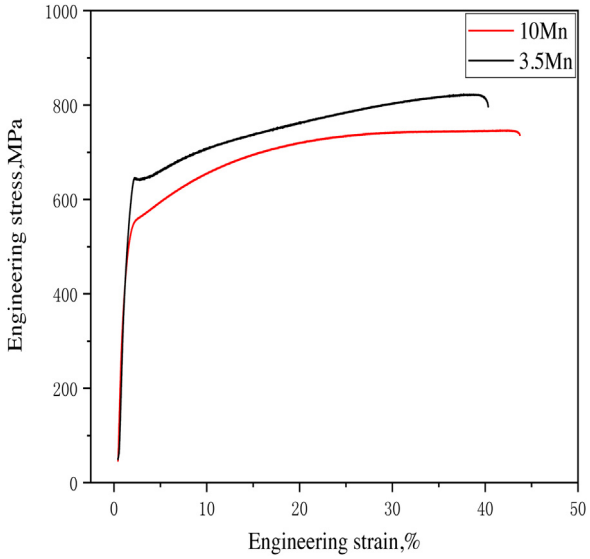

Fig. 5 – Engineering stress–strain curves of the steel investigated under quasi-static condition.

of austenite and a decrease in the carbon content in austenite, which results in a decrease in yield strength and tensile strength and an increase in elongation.

The fracture surface features of the steel tested under quasi-static condition were observed using SEM, shown in Fig. 6. Isometry dimples can be seen in the specimen, and the fracture form is a typical microporous aggregated ductile fracture. Both 3.5 Mn steel and 10 Mn steel have high plasticity. However, the dimple in 10 Mn steel is smaller and denser than the dimple in 3.5 Mn steel, so the elongation of 10 Mn steel is slightly better than that of 3.5 Mn steel.

The XRD patterns of the steel specimens before and after the quasi-static tensile testing are shown in Fig. 7. The volume fraction of austenite (Vγ) in 3.5 Mn steel before tensile deformation is 18%. The Vγ in the deformed microstructure is less than 5%. 72.2% of austenite produces phase transition. However, the volume fraction of austenite (Vγ) in 10 Mn steel before tensile deformation is 55%. The Vγ in the deformed microstructure is 43%. Only 21.8% of austenite produces phase transitions. The increase in Mn content enhances the stability of austenite, resulting in a smaller amount of austenite transformation. The research outputs [23–25] have shown that the deformation mechanism of austenite in steel is a main influential factor which determines steel properties. In order to study the strengthening mechanism of the steel investigated, it is necessary to firstly calculate the stacking fault energy.

In this study, the stacking fault energy of the steel studied is calculated by Eq. (2) according to Olson and Cohen [26].

$$SFE = 2\rho\Delta G_{\gamma\to\varepsilon} + 2\sigma_{\gamma/\varepsilon} \quad (2)$$

where ρ is the molar surface density determined by the {111} plane lattice constant, $\Delta G_{\gamma\to\varepsilon}$ is the molar Gibbs energy of the $\gamma\to\varepsilon$ phase transition; $\sigma_{\gamma/\varepsilon}$ is the γ/ε interface energy, which is 9 J/m^2. The chemical composition of austenite in lightweight steel sheet after holding at 850 °C for a period of time was calculated by Software Thermo-Calc using TCFE9 database. The stacking fault energy of 3.5 Mn steel calculated by Eq. (2) is 14.4 mJ m^{-2}, and the stacking fault energy of 10 Mn steel is 38 mJ m^{-2}. The previous research work [11] showed that, when the stacking fault energy was in the range of 20–40 mJ m^{-2}, it tended to obtain high strength, high plasticity and high strain hardening rate by forming mechanical twinning; when the stacking fault energy was in the range of 15–20 mJ m^{-2}, the TRIP effect and TWIP effect occurred simultaneously; when the stacking fault energy was less than 15 mJ m^{-2}, the martensitic transformation was the main deformation mechanism. Curtze and Kuokkala and Allain et al. [23–25] also indicated that stacking fault energy has a great influence on the deformation mechanism of Fe–C–Mn–Al steel. When the stacking fault energy is higher than 20 mJ m^{-2}, the deformation mechanism is TWIP effect dominant. While the stacking fault energy is less than 20 mJ m^{-2}, the deformation mechanism is TRIP effect dominant. In this study, the stacking fault energy of 3.5 Mn steel studied is less than 15 mJ m^{-2}, which should be dominated by the TRIP effect. However, the stacking fault energy of 10 Mn steel studied is more than 20 mJ m^{-2}, which should be dominated by the TWIP effect.

It can be seen in Fig. 8(a)-(c) that the austenite in 3.5 Mn lightweight steel is transformed into α′-martensite during the tensile deformation process at the stain-rate of 10^{-3}s^{-1}. The appearance of α′-martensite in the microstructure of the specimen after tensile deformation illustrates the existence of the TRIP effect indeed, which is consistent with the calculation results of the stacking fault energy. In Fig. 8(d)-(f), the austenite in 10 Mn lightweight steel is transformed into ε-martensite and deformation twin during the tensile deformation process at the stain-rate of 10^{-3} s^{-1}. The appearance of ε-martensite and deformation twin in the microstructure of the specimen after tensile deformation illustrates the existence of the TWIP effect indeed, which is also consistent with the calculation results of the stacking fault energy. Because of the TRIP and TWIP effect in austenite, both of the two steels have high strength, high elongation and excellent comprehensive performance.

3.3. *Tensile properties under dynamic loading conditions*

The engineering stress-strain curves of the steel investigated at different strain-rates are shown in Fig. 9. The mechanical properties of the two steels are listed in Table 3. With an increase in strain rate from 0.001 to 1200 s^{-1}, tensile strength of 3.5 Mn steel increases from 820 to 932 MPa. Yield strength

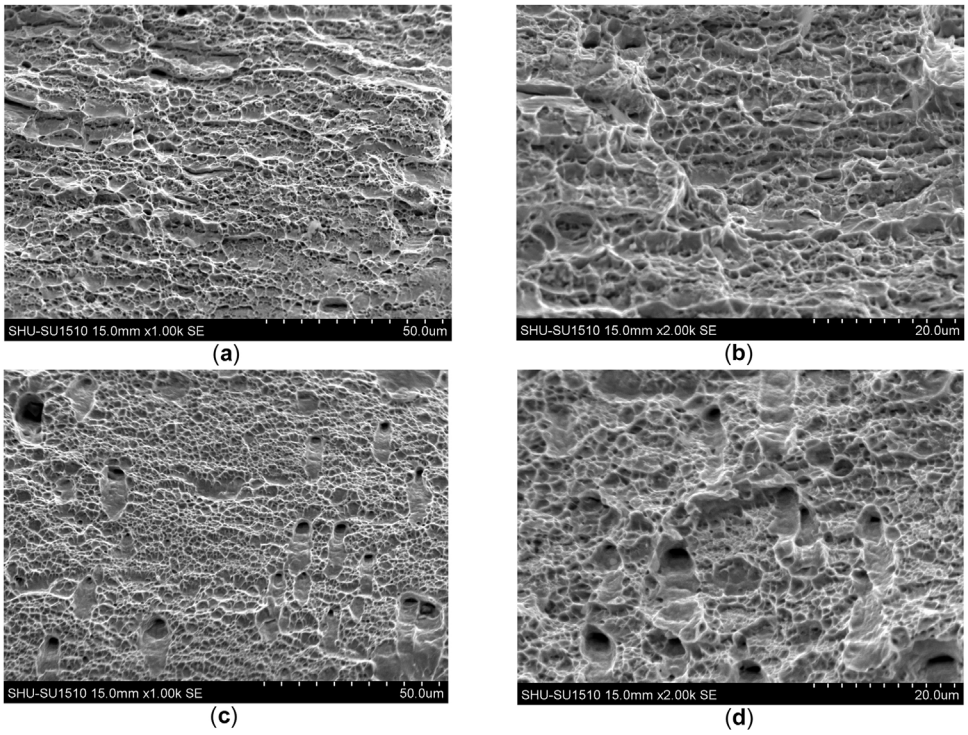

Fig. 6 – SEM Fracture morphology: (a) 1000 times of 3.5 Mn steel; (b) 2000 times of 3.5 Mn steel; (c) 1000 times of 10 Mn steel; (d) 2000 times of 10 Mn steel.

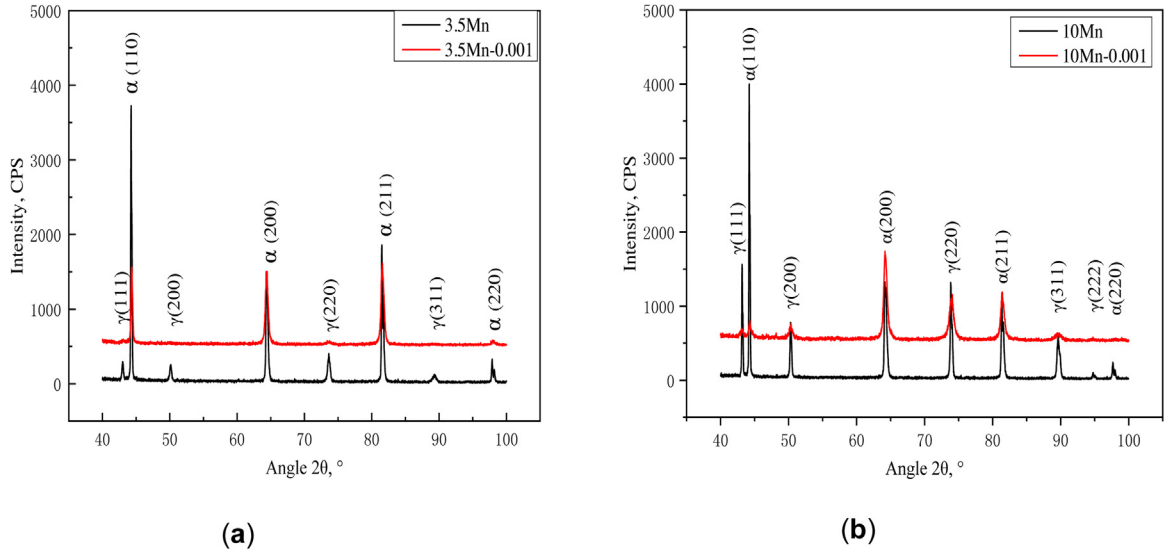

Fig. 7 – X-ray diffraction results of steel investigated before and after deformation: (a) 3.5 Mn steel; (b) 10 Mn steel.

increases from 640 to 806 MPa. Tensile strength of 10 Mn steel increases from 750 to 870 MPa. Yield strength increases from 570 to 747 MPa. Comparing with the quasi-static condition, yield strength of 3.5 Mn steel increases by 9.8, 24.2 and 25.9% and ultimate tensile strengths increases by 3.2, 10.5 and 13.7% respectively at the strain-rate of 5, 450 and 1200 s^{-1}. Yield strength of 10 Mn steel increases by 8.8, 26.0 and 31.1% and ultimate tensile strengths increases by 2.7, 12.0 and 16.0% respectively at the strain-rate of 5, 450 and 1200 s^{-1}. This is attributed to the large multiplication of dislocations in a short deformation time that makes the dislocation sliding difficult at the higher strain-rate [27,28]. The yield stage as initial stage of dislocation proliferation is significantly faster than the end stage of dislocation proliferation. However, with

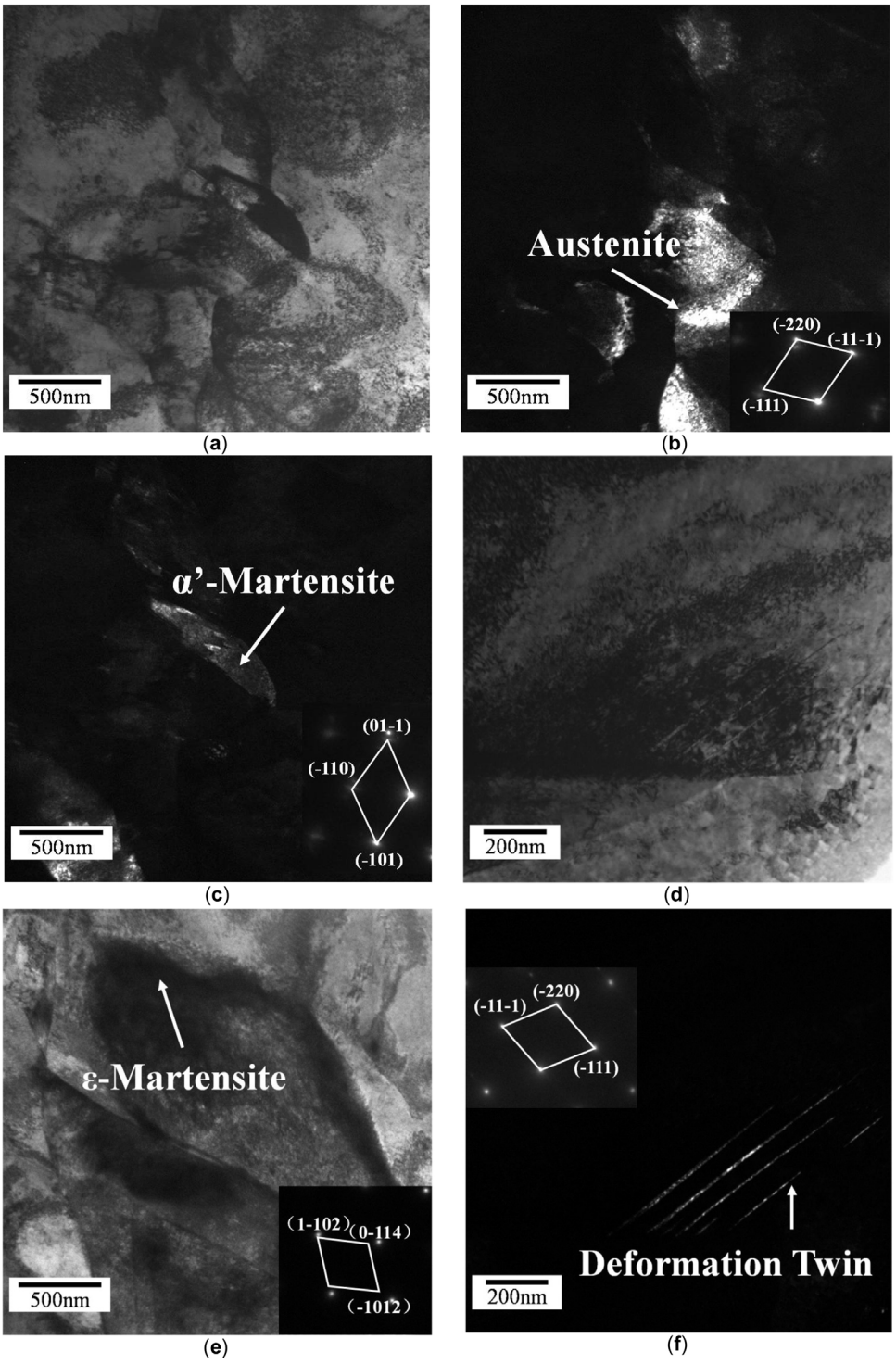

Fig. 8 – TEM analysis before and after deformation under quasi-static condition: (a) Bright field of 3.5 Mn steel; (b) Austenite and diffraction pattern of 3.5 Mn steel; (c) α′-martensite and diffraction pattern of 3.5 Mn steel; (d) Bright field of 10 Mn steel; (e) ε-martensite and diffraction pattern of 10 Mn steel; (f) Deformation twin and diffraction pattern of 10 Mn steel.

an increase in strain rate from 0.001 to 1200 s^{-1}, the elongation of 3.5 Mn steel studied initially decreases from 40 to 15%, and then increases from 16 to 29%. The elongation of 10 Mn steel studied initially decreases from 44 to 16%, and then increases from 16 to 29%. At a strain-rate of 450 s^{-1}, the elongation of the two steels are the minimal. It can be concluded that the plasticity-increasing effects in austenite induced by phase transformation or deformed twinning are suppressed by the deformation localization at a high strain-rate [29]. As the strain-rate increases to 1200 s^{-1}, it can be seen that the uniform elongation of the two steels start to increase. The possible reason is the softening of the matrix caused by adiabatic

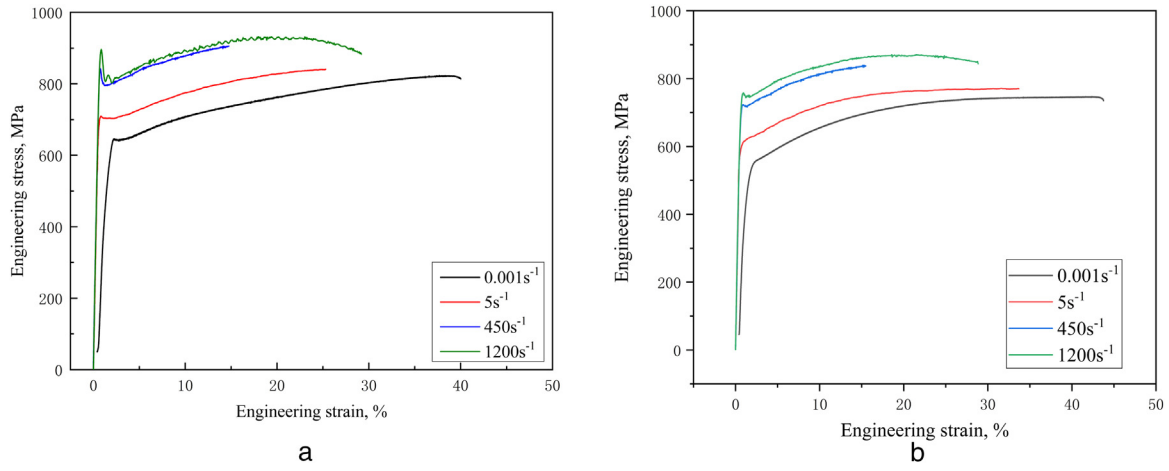

Fig. 9 – Tensile stress–strain curve at different strain rate: (a) 3.5 Mn steel; (b) 10 Mn steel.

Table 3 – Mechanical properties at different strain rate of two steels.

Steel	Strain rate	Yield strength (MPa)	Ultimate tensile strength (MPa)	Elongation (%)	Eab (MPa %)
3.5 Mn	0.001 s^{-1}	640	820	40	29,668
	5 s^{-1}	703	846	26	19,362
	450 s^{-1}	795	906	15	12,386
	1200 s^{-1}	806	932	29	25,868
10 Mn	0.001 s^{-1}	570	750	44	30,085
	5 s^{-1}	620	770	34	24,477
	450 s^{-1}	718	840	16	11,975
	1200 s^{-1}	747	870	29	23,903

heating. Adiabatic temperature can be calculated by Eq. (3) according to Curtze and Kuokkala [23].

$$\Delta T = \frac{\Delta Q}{\rho C_P} = \frac{\beta}{\rho C_p}\int_{\varepsilon_1}^{\varepsilon_2} \sigma d\varepsilon \tag{3}$$

where σ and ε indicate stress and strain, ρ is density, C_P is heat capacity, ΔT is temperature rise and β is the efficiency of the thermomechanical conversion. At a strain-rate of 1200 s^{-1}, ΔT of 3.5 Mn steel is 60 K and ΔT of 10 Mn steel is 65 K. Some related research [30,31] has shown that during deformation of AHSS(Advanced High Strength Steel), due to the changed work of plastic deformation and the latent heat caused by the phase transformation of the retained austenite, the temperature in the necking zone exceeds 80 °C at a strain-rate of 0.1 s^{-1}. Calculation results show that temperature at a strain-rate of 1000 s^{-1} increases almost by 100 °C.If the necking stage is considered, it could increase locally to over 300 °C. For that reason, the adiabatic heating has influenced the ductility of the two steels tested significantly by softening of matrix [32,33].

It is noted that the elongation of the two steels at the strain-rate of 1200 s^{-1} are always lower than that at the quasi-static condition. The reason is that the loss of ductility resulting from the weakness of the TRIP effect or TWIP effect is much greater than the benefit of ductility resulted from the softening of matrix caused by adiabatic heating.

For some automotive components, the ability to absorb energy is an important measurement index. In this research, integral areas of tensile curves are used to evaluate the capability of energy absorption [34], which are shown in Table 3. It can be seen that comparing with the quasi-static condition, the ultimate tensile strengths of 3.5 Mn lightweight steel at the strain-rate of 5, 450 and 1200 s^{-1} increase by 3.2, 10.5 and 13.7% respectively. However, the elongation of 3.5 Mn steel reduced by 35, 62.5 and 27.5%. The ultimate tensile strengths of 10 Mn lightweight steel at the strain-rate of 5, 450 and 1200 s^{-1} increase by 2.67, 12 and 16% respectively. However, the elongation of 10 Mn steel reduced by 22.7, 63.6 and 34.1%. The rate at which the tensile strength increases is not as fast as the elongation decreases, so comparing with the quasi-static condition, energy absorption of 3.5 Mn steel reduced by 34.7, 58.3 and 12.8% and energy absorption of 10 Mn steel reduced by 18.6, 60.2 and 20.5% respectively. It seems that at the strain-rate of 450 s^{-1}, energy absorption capacity of the two lightweight steels are the lowest.

Fig. 10 shows the results of X-ray diffraction. In Fig. 10(a), it can be seen that there is no obvious austenite peak at the strain-rate of 5 and 450 s^{-1}. Most retained austenite is transformed to α'-martensite. At the strain-rate of 0.001 s^{-1}, the volume fraction of austenite in 3.5 Mn steel is 4.36%. While at the strain-rate of 1200 s^{-1}, the volume fraction of austenite in the steel is 10.03%. More retained austenite does not transform to α'-martensite. It is concluded that adiabatic heating results in temperature rising in matrix, suppressed the transformation of austenite to martensite [35]. It is consistent with the conclusion of the literature [36]. At low strain rate, $\Delta\sigma$ (strength of ferrite relative to austenite) is relatively small, which enables the accommodation of plastic deforma-

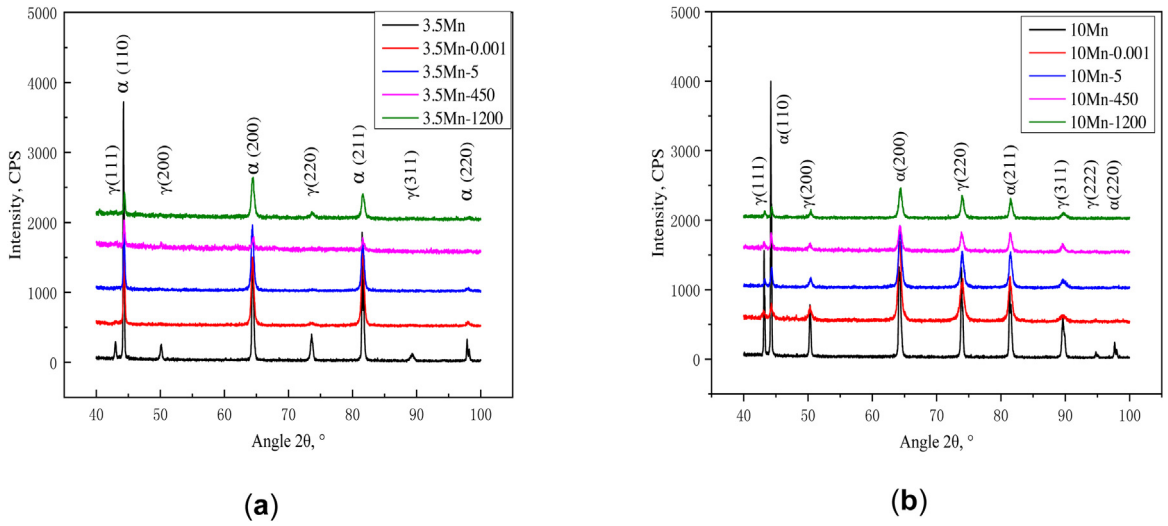

Fig. 10 – X-ray diffraction results before and after tensile fracture at different strain- rates: (a) 3.5 Mn steel; (b) 10 Mn steel.

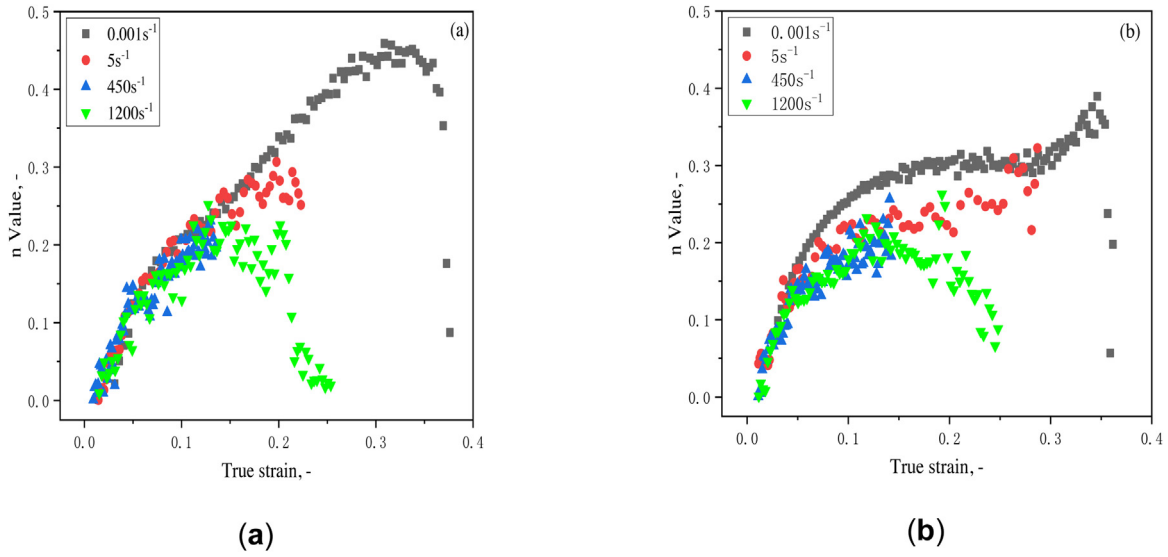

Fig. 11 – Instantaneous strain hardening exponent at strain rate of 0.001 s^{-1}, 5 s^{-1},450 s^{-1}, 1200 s^{-1}: (a) 3.5 Mn steel; (b) 10 Mn steel.

tion by ferrite and compensates the negative impact of the partial suppression of the TRIP effect. At medium strain rates, $\Delta\sigma$ is relatively high, and plastic deformation is primarily accommodated by austenite, which induces the pronounced activation of the TRIP mechanism. At high strain rate, plastic deformation is not accommodated by ferrite to a large extent due to a very high $\Delta\sigma$. Additionally, adiabatic heating effects partially suppress the TRIP effect in austenite. While in Fig. 10(b), there is no obvious change at the strain-rate of 0.001, 5, 450 and 1200 s^{-1}. It is concluded that the austenite in 10 Mn steel is more stable and adiabatic heating has little effect on deformation twin.

Fig. 11 is the curve of instantaneous strain hardening exponent (n value) with strain at different strain rates. It can be seen from the figure that in all deformation processes, the value of n increases from small to large, indicating that the dislocations in the material increase rapidly and the strain hardening effect becomes high. When the deformation is near the end, the strain hardening value increase rapidly, and then breakage occurs. While in Fig. 11(b), during the quasi-static tensile process, strain hardening value of one section is in a constant state. It is because that during the deformation process of 10 Mn steel, there is also stress relaxation at the same time of twinning strengthening, resulting in high plasticity. Although both two lightweight steels have austenite, the austenite in 3.5 Mn lightweight steel is obviously unstable and cannot provide progressive phase transition. At other strain rates of 10 Mn steel, there is no section where the strain hardening value is constant. The main reason is that the deformation speed is too fast, the material is not allowed to be slowly deformed, and it is too late to produce lax while the material is strengthened. By comparing the strain harden-

ing values at different strain rates, it is found that the strain hardening value decreases as the strain rate increases, which is consistent with the conclusion of the literature [37], and because the n value decreases, the sample will be broken before significant geometric necking occurred.

4. Conclusions

In this study, the influence of strain-rates and Mn content on the microstructure and mechanical properties of two lightweight steels have been studied in detail. Based on the research outcomes, the following conclusions can be drawn:

(1) At a strain-rate of 0.001 s^{-1} after annealing at 850 °C for 5 min then directly quenching into water, the ultimate tensile strength of 3.5 Mn lightweight steel is 820 MPa, the elongation is 40% and the product of strength and elongation (PSE) is 32,800 MPa %. The ultimate tensile strength of 10 Mn lightweight steel is 750 MPa, the elongation is 44% and the product of strength and elongation (PSE) is 33,000 MPa %. The two lightweight steels have a high strength and plasticity and exhibit excellent combinations of specific strength and ductility. During the tensile deformation process, the austenite in 3.5 Mn steel is transformed to α'-martensite. While in 10 Mn steel, the austenite is transformed to twinning.
(2) With an increase in strain rate from 0.001 to 1200 s^{-1}, tensile strength of 3.5 Mn steel increases from 750 to 870 MPa, whilst the elongation initially decreases from 44 to 16%, and then increases from 16 to 29%. Tensile strength of 10 Mn steel increases from 750 to 870 MPa, whilst the elongation initially decreases from 44 to 16%, and then increases from 16 to 29%. At the strain-rate of 450 s^{-1}, the elongation of the two lightweight steels are minimal, and the energy absorption capacity are the lowest.
(3) With the deformation progresses, the value of n increases from small to large, the strain hardening effect becomes high. With an increase in strain rate from 0.001 to 1200 s^{-1}, uniform deformation of 10 Mn lightweight steel was suppressed. Comparing with 10 Mn lightweight steel, the austenite in 3.5 Mn lightweight steel is obviously unstable and cannot provide progressive phase transition.

Conflicts of interest

The authors declare no conflicts of interest.

Acknowledgments

This work was financially supported by the National Key R&D Program of China under Grant 2017YFB0304402 and the Natural Science Research Foundation of China (No. 51801015)

REFERENCES

[1] Rana R, Liu C, Ray RK. Low-density low-carbon Fe–Al ferritic steels. Scripta Mater 2013;68:354–9.
[2] Renault C, Churyumov AY, Pozdniakov AV, Churyumov TA. Microstructure and hot deformation behavior of FeMnAlCMo steel. J Mater Res Technol 2020;9:4440–9.
[3] Mapelli C, Barella S, Gruttadauria A, Mombelli D, Bizzozero M, Veys X. γ Decomposition in Fe–Mn–Al–C lightweight steels. J Mater Res Technol 2020;9:4604–16.
[4] Liu D, Ding H, Cai M, Han D. Mechanical behaviors of a lower-Mn-added Fe–11Mn–10Al–1.25C lightweight steel with distinguished microstructural features. Mater Lett 2019;242:131–4.
[5] Suh DW, Kim NJ. Low-density steels. Scripta Mater 2013;68:337–8.
[6] Kang J, Li YJ, Wang XH, Wang HS, Yuan G, Misra RDK, et al. Design of a low density Fe–Mn–Al–C steel with high strength-high ductility combination involving TRIP effect and dynamic carbon partitioning. Mater Sci Eng A 2019;742:464–77.
[7] Sun B, Fazeli F, Scott C, Yan X, Liu Z, Qin X, et al. Critical role of strain partitioning and deformation twinning on cracking phenomenon occurring during cold rolling of two duplex medium manganese steels. Scripta Mater 2017;130:49–53.
[8] Lee S, Shin S, Kwon M, Lee K, De Cooman BC. Tensile properties of medium Mn steel with a bimodal UFG α + γ and coarse δ-ferrite microstructure. Metall Mater Trans A 2017;48:1678–700.
[9] Frommeyer G, Brux U. Microstructures and mechanical properties of high-strength Fe–Mn–Al–C light-weight TRIPLEX steels. Steel Res Int 2006;7:627–33.
[10] Sun B, Fazeli F, Scott C, Brodusch N, Gauvin R, Yue S. The influence of silicon additions on the deformation behavior of austenite-ferrite duplex medium manganese steels. Acta Mater 2018;148:249–62.
[11] Grassel O, Krueger L, Frommeyer G, Mever LW. High strength Fe–Mn–(Al, Si) TRIP/TWIP steels development properties application. Int J Plast 2000;16:1391–409.
[12] Sohn SS, Song H, Suh BC, Kwak JH, Lee BJ, Kim NJ, et al. Novel ultra-high-strength (ferrite + austenite) duplex lightweight steels achieved by fine dislocation substructures (Taylor lattices), grain refinement, and partial recrystallization. Acta Mater 2015;96:301–10.
[13] Zhang M, Cao W, Dong H, Zhu J. Element partitioning effect on microstructure and mechanical property of the micro-laminated Fe–Mn–Al–C dual phase steel. Mater Sci Eng A 2016;654:193–202.
[14] Cheng WC, Cheng CY, Hsu CW, Laughlin DE. Phase transformation of the L1 2 phase to kappa-carbide after spinodal decomposition and ordering in an Fe–C–Mn–Al austenitic steel. Mater Sci Eng A 2015;642:128–35.
[15] Moon J, Park SJ, Jang JH, Lee TH, Lee CH, Hong HU, et al. Atomistic investigations of κ-carbide precipitation in austenitic Fe–Mn–Al–C lightweight steels and the effect of Mo addition. Scripta Mater 2017;127:97–101.
[16] Rahman KM, Vorontsov VA, Dye D. The dynamic behaviour of a twinning induced plasticity steel. Mater Sci Eng A 2014;589:252–61.
[17] Park J, Kang M, Sohn SS, Kim SH, Kim SH, Kim NJ, et al. Quasi-static and dynamic deformation mechanisms interpreted by microstructural evolution in TWinning Induced Plasticity (TWIP) steel. Mater Sci Eng A 2017;684:54–63.
[18] Tang ZY, Misra RDK, Ma M, Zan N, Wu ZQ, Ding H. Deformation twinning and martensitic transformation and dynamic mechanical properties in Fe–0.07C–23Mn–3.1Si–2.8Al TRIP/TWIP steel. Mater Sci Eng A 2015;624:186–92.
[19] Ha Y, Kim H, Kwon KH, Lee SG, Lee S, Kim NJ. Microstructural evolution in Fe–22Mn–0.4C twinning-induced plasticity steel

during high strain rate deformation. Metall Mater Trans A 2014;46:545–8.
[20] Wu H, Ma G, Xia Y. Experimental study of tensile properties of PMMA at intermediate strain rate. Mater Lett 2004;58:3681–5.
[21] He Z, He Y, Ling Y, Wu Q, Gao Y, Li L. Effect of strain rate on deformation behavior of TRIP steels. J Mater Process Technol 2012;212:2141–7.
[22] Dyson DJ. Effect of alloying additions on the lattice parameter of austenite. J Iron Steel Inst 1970;208:469–74.
[23] Curtze S, Kuokkala VT. Dependence of tensile deformation behavior of TWIP steels on stacking fault energy, temperature and strain rate. Acta Mater 2010;58: 5129–41.
[24] Allain S, Chateau JP, Bouaziz O. A physical model of the twinning-induced plasticity effect in a high manganese austenitic steel. Mater Sci Eng A 2004;387:143–7.
[25] Allain S, Chateau JP, Bouaziz O, Migot S, Guelton N. Correlations between the calculated stacking fault energy and the plasticity mechanisms in Fe–Mn–C alloys. Mater Sci Eng A 2004;387–389:158–62.
[26] Olson GB, Cohen M. A general mechanism of martensitic nucleation: part I. General concepts and the FCC → HCP transformation. Metall Trans A 1976;7:1897–904.
[27] Ryttberg K, Knutson Wedel M, Dahlman P, Nyborg L. Microstructural evolution during fracture induced by high strain rate deformation of 100Cr6 steel. J Mater Process Technol 2009;209:3325–34.
[28] Xu S, Ruan D, Beynon JH, Rong Y. Dynamic tensile behaviour of TWIP steel under intermediate strain rate loading. Mater Sci Eng A 2013;573:132–40.
[29] Colas R, Grinberg A. A study of strain localization by means of reduced gage compression testing. J Mater Process Technol 1999;88:276–83.
[30] Li D, Wei Y, Liu C, Hou L, d Liu, Jin X. Effects of high strain rate on properties and microstructure evolution of TWIP steel subjected to impact loading. J Iron Steel Res Int 2010;17:7.
[31] Gronostajski Z, Niechajowicz A, Kuziak R, Krawczyk J, Polak S. The effect of the strain rate on the stress- strain curve and microstructure of AHSS. J Mater Process Technol 2017;242:246–59.
[32] Gao Y, Xu C, He ZP, Yl He, Li L. Response characteristics and adiabatic heating during high strain rate for TRIP steel and DP steel. J Iron Steel Res Int 2015;22:48–54.
[33] Li X, Chen L, Zhao Y, Misra RDK. Influence of manganese content on ε-/α'-martensitic transformation and tensile properties of low-C high-Mn TRIP steels. Mater Des 2018;142:190–202.
[34] Kang M, Park J, Sohn SS, Ahn DH, Kim HS, Cho WT, et al. Dynamic tensile behavior of twinning-induced plasticity/low-carbon (TWIP/LC) steel clad sheets bonded by hot rolling. Mater Sci Eng A 2017;700:387–96.
[35] Wei X, Fu R, Li L. Tensile deformation behavior of cold-rolled TRIP-aided steels over large range of strain rates. Mater Sci Eng A 2007;465:260–6.
[36] Sevsek S, Haase C, Bleck W. Strain-rate-dependent deformation behavior and mechanical properties of a multi-phase medium-manganese steel. Metals 2019;9:344–65.
[37] Tang C, Zhu J, Zhang Y, Zhou H. Effect of strain rate on strain hardening exponent of some metallic materials. Acta Metall Sin 1994;7:183–6.